Nonlinear Dynamics (2026)114:362
https://doi.org/10.1007/s11071-026-12241-0

RESEARCH

Scattering of coupled particles on a potential well

Yam Aksenton[1] · Attila Genda[2] · Oleg V. Gendelman[1] · Alexander Fidlin[2]

Received: 11 September 2025 / Revised: 2 December 2025 / Accepted: 7 January 2026

Abstract
This paper investigates the dynamics of scattering of a 2DOF system of coupled particles on a potential well. In the considered one-dimensional setting, the system can either pass through the well or rebound. If dissipative effects are included, another possible outcome is the system's trapping in the well. The scattering outcomes are intrinsically related to the energy transfer mechanisms between the coupled system and the well. For some initial conditions, one observes an extremely sensitive (chaotic-like) dependence of the scattering outcome. Relatively large initial velocities of the system or a relatively small free length of the internal coupling allow for an asymptotic approach and analytical prediction of the scattering outcomes and parameters. In particular, it is possible to predict the residual amplitudes of the oscillations of the coupled system and the transition to sensitive (chaotic-like) dynamics. The developed approaches and observed scattering patterns seem generic and applicable to a wide variety of similar models.

Keywords Scattering · Energy transfer

1 Introduction

The notion of a potential well has a wide range of applications in science and engineering. For example, in chemistry, potential wells are a traditional tool for modelling chemical reactions [1]. The dynamics of MEMS and energy harvesters [2, 3] often invoke potential wells for the formulation of simplified mathematical models [3–5]. In the field of MEMS, one also usually analyzes the non-stationary dynamics in potential wells for the description of the actuation modalities [6, 7]. Potential wells also profoundly appear in simplified versions of the famous three-body problem [8, 9] and more general issues of celestial dynamics [10]. Escape and transition dynamics of basic model systems with potential wells are the subject of many recent research efforts [11–15]. These types of problems can often be solved with perturbation theory and asymptotic analysis [16].

This research focuses on the situation opposite to escape. We consider the motion of coupled particles that arrive in the vicinity of the potential well and scatter on it. For a single-DOF system, the basic problem of scattering (or trapping) is quite simple. If damping is absent, the particle overcomes the potential well or rebounds from the potential barrier; these outcomes are simply related to the initial energy. When damping is present, the problem becomes more challenging, and trapping becomes possible, but it can still be fully described in terms of dynamics on the state plane. In a coupled system of two or more particles, one should consider the possibility of energy exchange between the modes of the system, induced by its interaction with the well. The current paper addresses precisely this challenge for a simple system of linearly coupled identical particles along one spatial dimension. Additional examples of articles exploring scattering in the interaction of bodies or particles are given in [17–20].

The structure of the paper is as follows. Section 2 is devoted to the description of the model. Section 3 contains a numerical exploration of conservative and damped cases. In the conservative case, due to conservation of the phase volume, the coupled system, initially placed outside the well always ends up outside the well; thus, possible scattering outcomes are transition (passage) over the well or reflection (rebound). If linear viscous damping acts

✉ Oleg V. Gendelman
ovgend@technion.ac.il

[1] Faculty of Mechanical Engineering, Technion – Israel Institute of Technology, Haifa, Israel

[2] Karlsruhe Institute of Technology, Karlsruhe, Germany

Published online: 10 March 2026

between the particles, the system may become trapped inside the well. Section 4 includes an analytic treatment of some regularities observed in the numerical simulations and presents predictions for the amplitude of residual oscillations and, most importantly, for the transition between different scattering regimes. Section 5 includes a discussion and concluding remarks.

2 Model description

A sketch of the explored system is presented in Fig. 1.

The system investigated in this paper consists of two identical particles of mass m. Without loss of generality, we choose the non-dimensional value $m = 1$. The particles are coupled by a linear spring of stiffness k and free length l_0 (the length at which the spring is relaxed). We assume linear viscous damping with a damping coefficient c acting between the particles. Initially, the particles are located on the right-hand side of the potential well, far enough from its center, to remain almost unaffected by the well's attraction. The particles are given the same initial velocity u_0, pointing towards the center of the well. A somewhat similar system was considered in [21] to analyze escape rather than scattering. The model potential used in the subsequent analysis is given in Eq. (1) and depicted graphically in Fig. 2.

$$V(x) = -\frac{1}{2\cosh^2(x)} \tag{1}$$

This smooth model potential was chosen because it rapidly (exponentially) converges to a finite value at $\pm\infty$. Therefore, it is reasonable to explore the scattering problem if the system is initially placed far from the potential well.

All quantities are expressed in non-dimensional form in accordance with the characteristic scales of the potential. Around $x = 0$, the potential equation can be approximated as:

$$V(x) \approx \frac{1}{2}x^2 - \frac{1}{2} \tag{2}$$

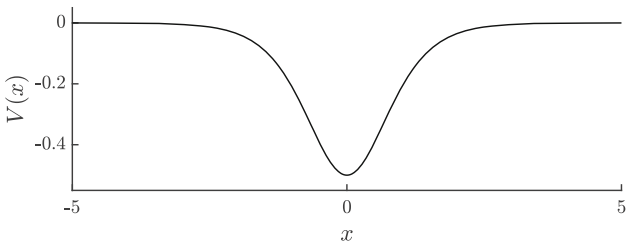

Fig. 2 The underlying potential well

It corresponds to a natural frequency of $\omega_0 = 1$. Then, the time is scaled with $\frac{1}{\omega_0}$, and the coupling force stiffness k is then a non-dimensional parameter.

The spatial coordinate x_i and the free length parameter l_0 are likewise scaled through the characteristic depth of $V(x)$, defined by its minimum value of $-\frac{1}{2}$.

The total non-dimensional energy of the system is given as follows:

$$E = \frac{1}{2}\left(\dot{x}_1^2 + \dot{x}_2^2\right) + \frac{1}{2}k(x_1 - x_2 + l_0)^2 + V(x_1) + V(x_2) \tag{3}$$

The dissipation function takes the form

$$G = \frac{1}{2}c(\dot{x}_1 - \dot{x}_2)^2 \tag{4}$$

The resulting equations of motion are given by

$$\begin{cases} \ddot{x}_1 + c(\dot{x}_1 - \dot{x}_2) + k(x_1 - x_2 + l_0) = -\left.\dfrac{\partial V}{\partial x_1}\right|_{x_1} \\ \ddot{x}_2 - c(\dot{x}_1 - \dot{x}_2) - k(x_1 - x_2 + l_0) = -\left.\dfrac{\partial V}{\partial x_2}\right|_{x_2} \end{cases} \tag{5}$$

The non-dimensional parameters that will be explored throughout the analysis in the paper are the stiffness k, the free length l_0 and the initial velocity u_0.

2.1 The 1DOF system as a reference case

To achieve a better understanding of the system, one must first consider the scattering dynamics of a single particle with the same potential. The conservative equation of motion for the 1DOF system is written as follows:

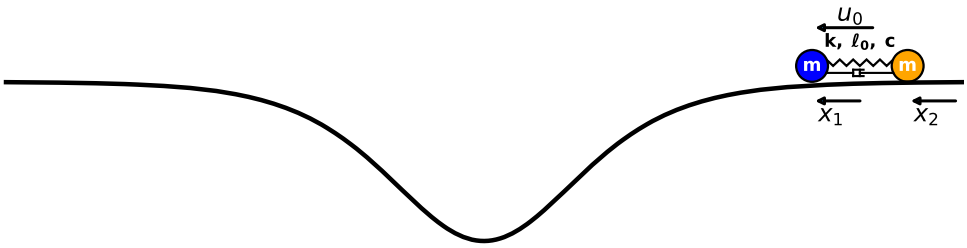

Fig. 1 Sketch of the problem setting

$$\ddot{x}+\frac{\partial V}{\partial x}=0;\ V(x)=\frac{-1}{2\cosh^2(x)} \tag{6}$$

For $E<0$, the particle remains inside the potential, and all its trajectories perform periodic oscillations that remain bounded within the well.

For $E>0$, the motion is unbounded, and all trajectories diverge to $|x|\to\infty$.

At $E=0$, the particle's motion lies on a separatrix connecting the points at infinity. in that case, the velocity tends to zero as $|x|\to\infty$.

Additional dissipation leads to the modification of these outcomes, depending on the specific model of dissipation. For a linear damping $c\dot{x}$, it is well known that the particle arrives at zero velocity after travelling a certain finite distance, even without the external potential. The increasing external potential function can only facilitate this stop as it causes additional energy loss. Thus, the velocity of the particle becomes zero for some finite coordinate. It means that for any initial condition for a given potential function, all trajectories converge to the single stable equilibrium at $x=0$, and no scattering toward $|x|\to\infty$ is possible. As will be demonstrated below, the gradient coupling in 2DOF systems can lead to a family of qualitatively different outcomes.

3 Numerical results

The numerical analysis is divided into two parts: the first for the undamped, conservative system; the second for the damped, non-conservative one. The simulations are performed for a broad set of parameters to gain insight into the general properties of the model. Special attention is paid to limit cases of large stiffness, small and large initial velocities, and small free lengths that allow for asymptotic analysis.

3.1 Conservative system

The system is undamped ($c=0$), meaning the total energy is unchanged. According to Liouville's theorem, when energy is conserved, the trajectory of the system cannot remain bounded within the well, as its energy exceeds the difference between the well bottom and its asymptotic value. The equations of motion of the undamped system are written as follows:

$$\begin{cases}\ddot{x}_1=-k(x_1-x_2+l_0)-\left.\dfrac{\partial V}{\partial x_1}\right|_{x_1}\\ \ddot{x}_2=k(x_1-x_2+l_0)-\left.\dfrac{\partial V}{\partial x_2}\right|_{x_2}\end{cases} \tag{7}$$

3.1.1 Types of scattering for different parameters

The maps of different scattering outcomes for various sets of parameters are depicted in Fig. 3

Some features of the scattering maps should be underlined. First, some regions of the map are *robust*, i.e., large regions of parameters result in the same scattering outcome. Primarily, such extended, connected regions characterize the transition through the well. Second, other regions are *sensitive*, i.e., they include a mixture of points with different outcomes. We can say that for these sets of parameters, the outcomes sensitively depend on the initial conditions, somewhat similar to sensitive responses in excited dynamical systems. One obvious observation is that as the initial velocity increases, the system tends to pass over the well. Similar trends are observed as l_0 decreases and k increases. To further expand our understanding of the sensitive areas, a heat map of the time the system lingers inside the well is presented in Fig. 4.

It is noticeable how sensitive areas correspond identically in both Figs. 3 and 4, and that in those sensitive areas, the system tends to remain inside the well for a much longer time period, increasing the well's effect on the particles and resulting in further amplification in the exchange of energy between the modes. These observations are used below in the asymptotic analysis.

3.1.2 Residual oscillations after scattering

Far from the well's center, the contribution of potential energy to the total energy can be neglected, and the equations of motion are reduced to the following form:

$$\begin{cases}\ddot{x}_1+k(x_1-x_2+l_0)=0\\ \ddot{x}_2-k(x_1-x_2+l_0)=0\end{cases} \tag{8}$$

It is convenient to switch to the center of mass (COM) R and the relative displacement w variables:

$$\begin{cases}R=\dfrac{1}{2}(x_1+x_2)\\ w=(x_1-x_2+l_0)\end{cases} \tag{9}$$

The equations of motion for the new coordinates take the form:

$$\begin{cases}\ddot{w}+2c\dot{w}+2kw=\left.\dfrac{\partial V}{\partial x_2}\right|_{R-\frac{w}{2}+\frac{l_0}{2}}-\left.\dfrac{\partial V}{\partial x_1}\right|_{R+\frac{w}{2}-\frac{l_0}{2}}\\ \ddot{R}=-\dfrac{1}{2}\left(\left.\dfrac{\partial V}{\partial x_1}\right|_{R+\frac{w}{2}-\frac{l_0}{2}}+\left.\dfrac{\partial V}{\partial x_2}\right|_{R-\frac{w}{2}+\frac{l_0}{2}}\right)\end{cases} \tag{10}$$

The equations are then reduced in the scattered state to an even simpler form:

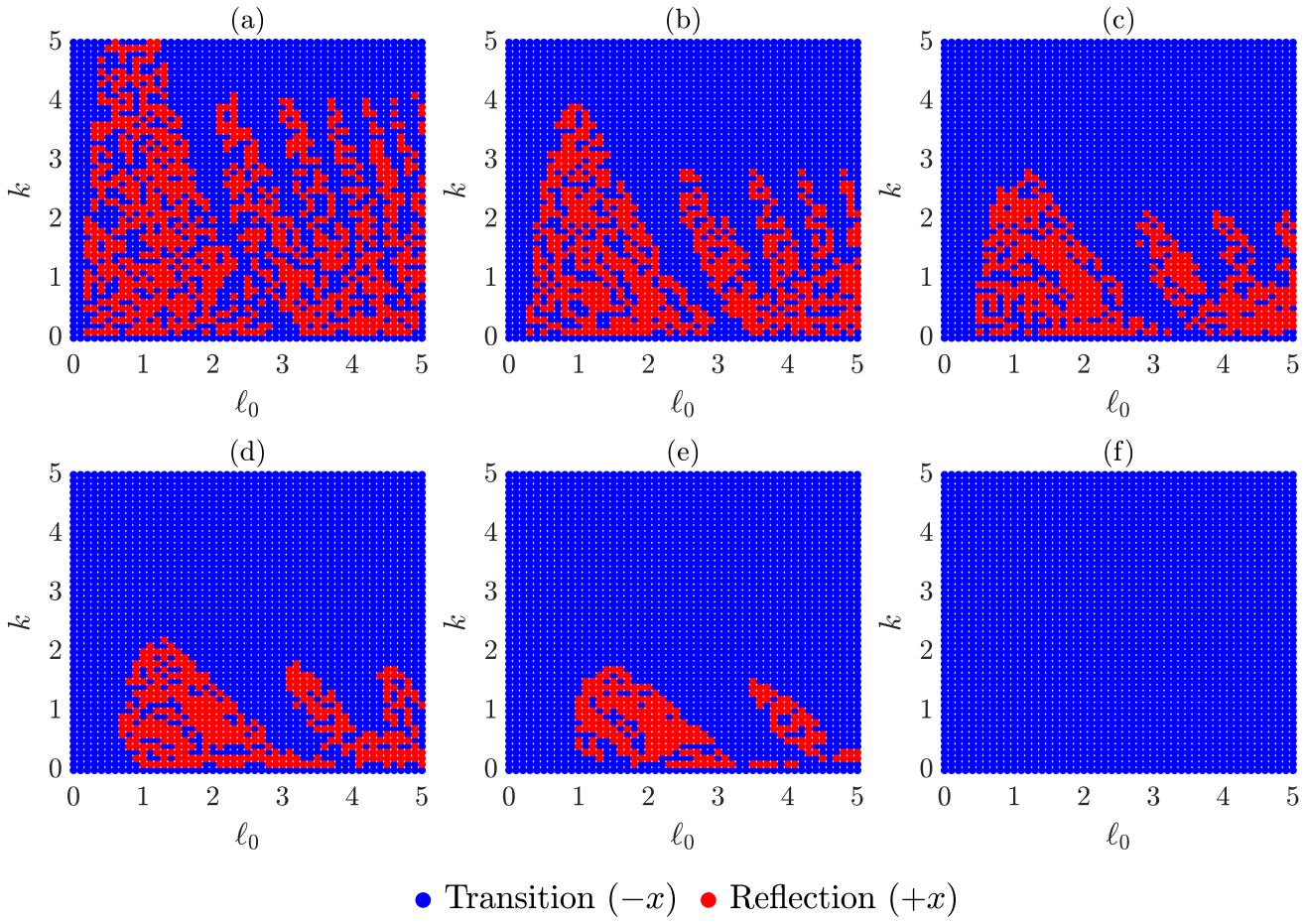

Fig. 3 Scattering maps for various sets of parameters. The spring's free length l_0 is shown along the horizontal axis, while the spring stiffness k corresponds to the vertical axis for the following initial velocity values: **a** $u_0 = -0.1$ **b** $u_0 = -0.2$ **c** $u_0 = -0.3$ **d** $u_0 = -0.4$ **e** $u_0 = -0.5$ **f** $u_0 = -1$

$$\begin{cases} \ddot{w} + 2kw = 0 \\ \ddot{R} = 0 \end{cases}. \tag{11}$$

The equation for the relative displacement coordinate w matches that of a simple harmonic oscillator, with a frequency of $\sqrt{2k}$, whereas the amplitude of the residual oscillations depends on the scattering history. The following figures present how the residual amplitudes depend on the initial velocity; the scattering outcome is also marked (see Fig. 5). The spring's stiffness varies between each graph, while its free length remains constant.

The first interesting and somewhat unexpected observation from Fig. 5 is the *non-monotonic dependence* of the residual amplitude on the initial velocity. In addition, the system becomes less sensitive as the stiffness increases. The same trend is observed for larger values of initial velocity, accompanied by a sharp decrease in amplitude.

Figure 6 presents a graph with similar amplitudes with the initial velocity as the running parameter. This time, the free length varies between each graph while the stiffness remains constant.

Based on Fig. 6, we can conclude that a reduction in free length values yields less sensitive behavior. The non-monotonicity also clearly reveals itself. The conclusion from Fig. 5 about smaller amplitudes at large velocities is relevant in Fig. 6 as well.

3.2 Non-conservative system

When the damping is included, the system obtains a new possible scattering outcome – trapping. Some typical scattering maps are presented in Fig. 7.

Figure 7 presents the scattering map for relatively low initial energy in the system, for various damping coefficients. One can note that the parametric regions that are sensitive in the case of zero damping (Fig. 7a) turn into trapping regions even for very small damping (Fig. 7b and further). The effect of trapping in sensitive areas can be explained by the prolonged lingering of the system inside the well, observed in these areas in Fig. 4. The system's

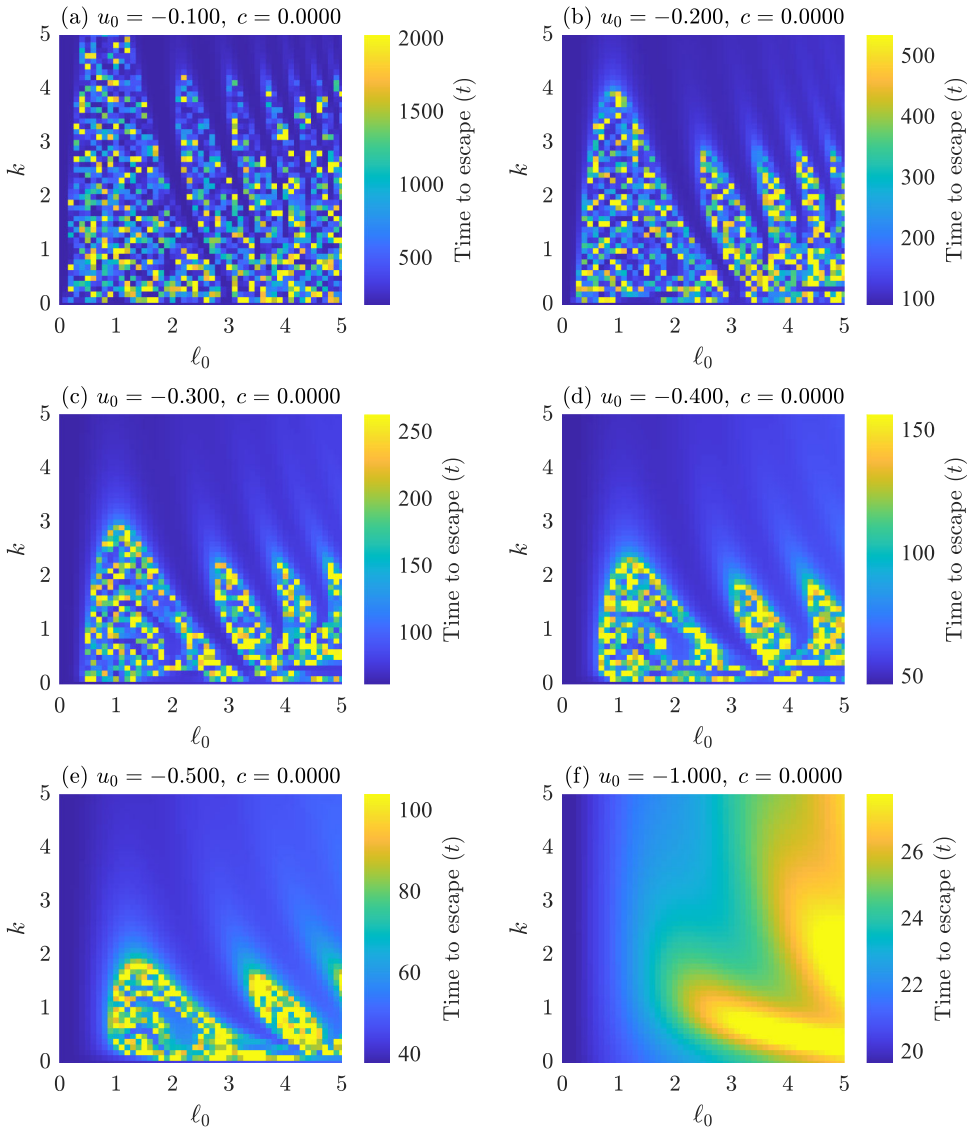

Fig. 4 Heat map of the duration the system lingers inside the well for different initial velocities. The horizontal axis represents the free length l_0, while the vertical axis represents the spring stiffness k. The initial velocity values are as follows: **a** $u_0 = -0.1$ **b** $u_0 = -0.2$ **c** $u_0 = -0.3$ **d** $u_0 = -0.4$ **e** $u_0 = -0.5$ **f** $u_0 = -1$

lingering in the well results in the intensification of energy exchange into the relative displacement mode w, in which energy is dissipated. The reflection outcome eventually disappears, even for rather modest damping values. Interestingly, for relatively high damping, the transition outcome reappears – presumably, due to the effective stiffening of the system (Fig. 7f).

4 Asymptotic analysis for the conservative case

The numerical analysis provided valuable findings that aid in identifying treatable cases where the system exhibits robust behaviors. Two important observations in robust regimes to be considered in the study are the negligible amplitudes of residual oscillations and the guaranteed transition of the system.

4.1 Approximation of large velocities

The initial energy is concentrated solely in the COM mode of motion (R). Energy transfer between modes occurs once the system enters the vicinity of the well. The energy expression in (3) can be rewritten using modal coordinates:

$$E = \dot{R}^2 + \frac{\dot{w}^2}{4} + \frac{1}{2}kw^2 - \frac{1}{2\cosh^2\left(R + \frac{w}{2} - \frac{l_0}{2}\right)} - \frac{1}{2\cosh^2\left(R - \frac{w}{2} + \frac{l_0}{2}\right)} \tag{12}$$

The energy expression can be further simplified by neglecting the amplitude of residual oscillations, as mentioned earlier:

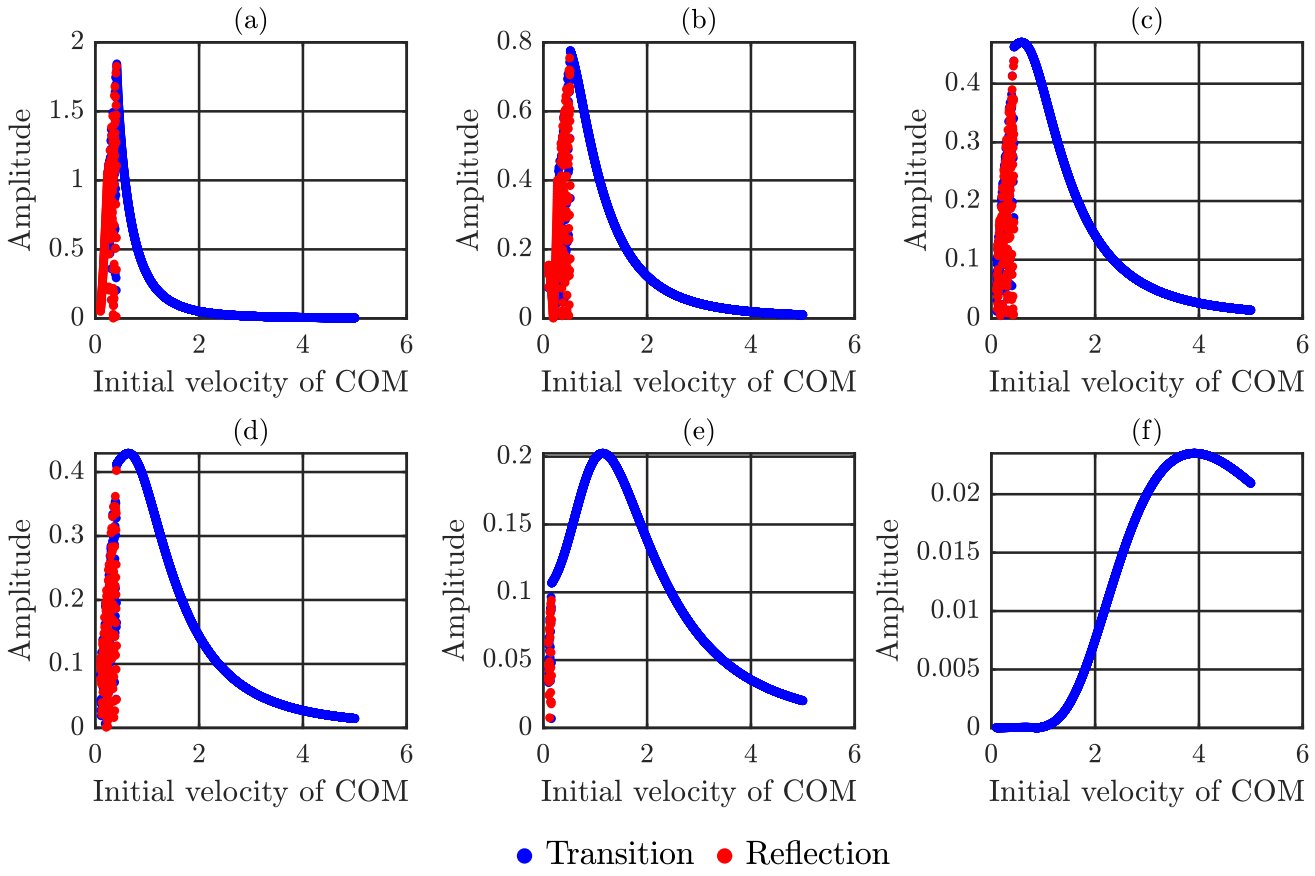

Fig. 5 Amplitudes of residual oscillations over the initial velocity, for a constant free length $l_0 = 1$ and various stiffness values: **a** $k = 0.1$ **b** $k = 0.9$ **c** $k = 1.8$ **d** $k = 4.5$ **e** $k = 8$ **f** $k = 40$

$$E = \dot{R}^2 - \frac{1}{2\cosh^2\left(R - \frac{l_0}{2}\right)} - \frac{1}{2\cosh^2\left(R + \frac{l_0}{2}\right)} \tag{13}$$

The phase portrait of the energy equation in Fig. 8 demonstrates the diminishing effect of the potential well on the velocity of the COM ($\dot{R}$) as the initial energy increases. It means that large initial velocities cause the system to move at an almost constant velocity, effectively 'hovering' over the well:

$$\dot{R} \approx u_0 \tag{14}$$

Under this conclusion and the assumption of a small residual oscillation amplitude, one can make the following approximations to the modal equations of motion:

$$\begin{cases} \ddot{w} + 2kw = \left.\dfrac{\partial V}{\partial x_2}\right|_{x_{1\_0}+u_0 t+\frac{l_0}{2}} - \left.\dfrac{\partial V}{\partial x_1}\right|_{x_{1\_0}+u_0 t-\frac{l_0}{2}} . \\ \ddot{R} = 0 \end{cases} \tag{15}$$

The solution for the relative displacement is obtained through a simple convolution (for the complete derivation, see the Appendix, Sect. 6.1):

$$w(t) = \frac{\pi\sqrt{2k}}{u_0^3 \sinh\left(\frac{\pi\sqrt{2k}}{2u_0}\right)} \sin\left(\frac{\sqrt{2k}l_0}{2u_0}\right) \sin\left(\sqrt{2k}t + \frac{\sqrt{2k}}{u_0}\left(x_{1\_0} + \frac{l_0}{2}\right)\right) \tag{16}$$

The amplitude expression is then simply extracted as:

$$amp(w) = \frac{\pi\sqrt{2k}}{u_0^3 \sinh\left(\frac{\pi\sqrt{2k}}{2u_0}\right)} \sin\left(\frac{\sqrt{2k}l_0}{2u_0}\right) \tag{17}$$

4.2 Approximations for small free lengths

Smaller free lengths also proved to yield robust results in the numerical section and provided a guaranteed transition. By utilizing this observation and neglecting the amplitude of residual oscillations in the argument of the $\cosh^2(\cdot)$ function, the modal energy equation can be reformulated in the following manner:

$$E = \dot{R}^2 - \frac{1}{\cosh^2(R)} \tag{18}$$

Considering that both particles initialize with the same velocity u_0, and that energy is conserved throughout the

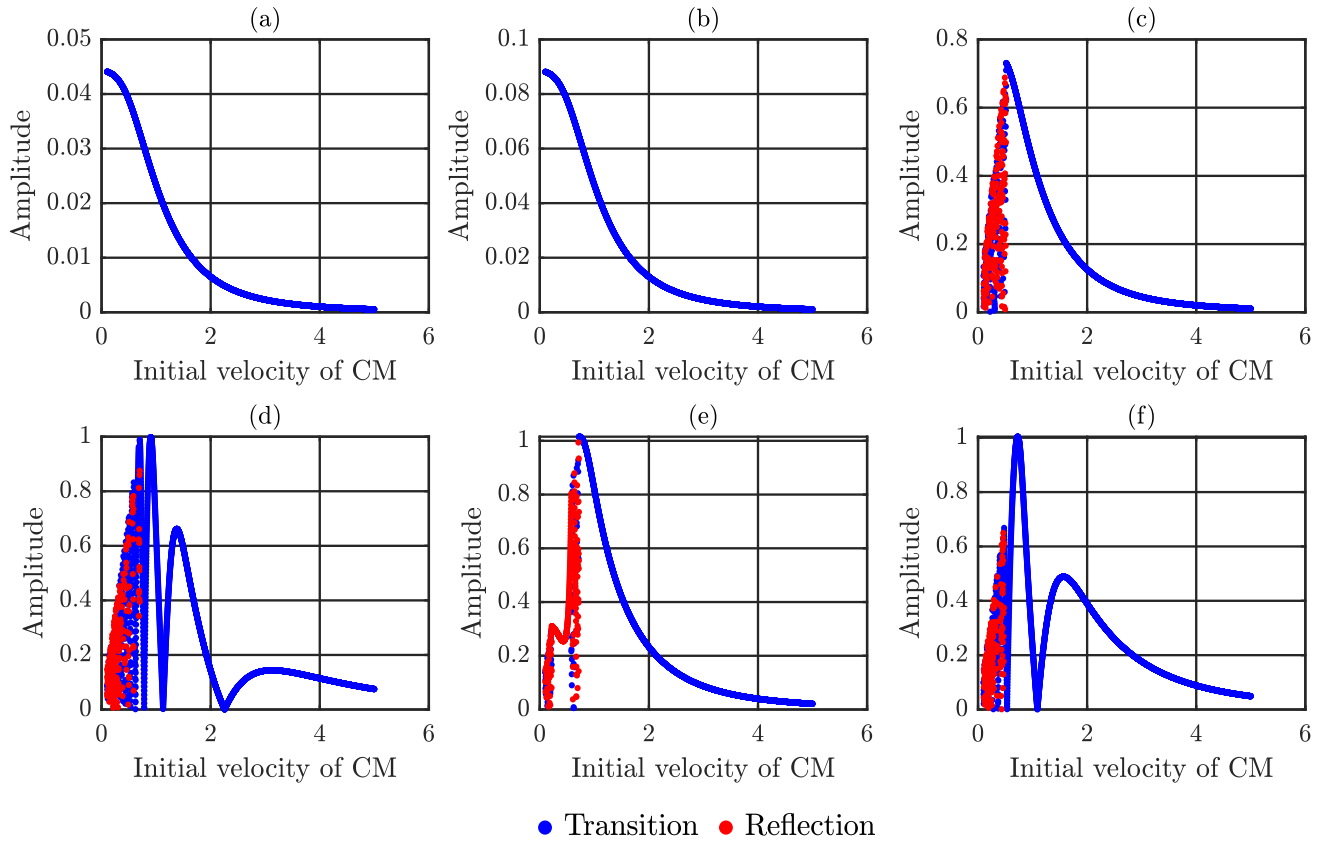

Fig. 6 Amplitude of residual oscillations over initial velocity, for constant stiffness $k = 1$ and differing free length values: **a** $l_0 = 0.05$ **b** $l_0 = 0.1$ **c** $l_0 = 1$ **d** $l_0 = 2$ **e** $l_0 = 5$ **f** $l_0 = 10$

motion of the system, the total energy of the system is calculated as:

$$E = u_0^2 \equiv const \tag{19}$$

Equations 18 is an ODE with a full analytic solution (for the complete derivation see the Appendix, Sect. 6.2):

$$R = \operatorname{arcsinh}\left(\sqrt{\frac{E+1}{E}} \cdot \sinh\left(-t\sqrt{E} + \operatorname{arcsinh}\left(\frac{\sinh\left(x_{1\_0} + \frac{l_0}{2}\right)}{\sqrt{E+1}}\right)\right)\right) \tag{20}$$

Expression (18) is inserted into the ODE of the relative displacement in Eq. (10) yielding

$$\ddot{w} + 2kw = -\frac{\sinh\left(R + \frac{l_0}{2}\right)}{\cosh^3\left(R + \frac{l_0}{2}\right)} + \frac{\sinh\left(R - \frac{l_0}{2}\right)}{\cosh^3\left(R - \frac{l_0}{2}\right)} \tag{21}$$

When considering the small free length value, the term on the RHS takes the form:

$$\lim_{l_0 \to 0}\left(\frac{\sinh\left(R - \frac{l_0}{2}\right)}{\cosh^3\left(R - \frac{l_0}{2}\right)} - \frac{\sinh\left(R + \frac{l_0}{2}\right)}{\cosh^3\left(R + \frac{l_0}{2}\right)}\right) = l_0 \frac{\partial}{\partial R}\left(\frac{\sinh(R)}{\cosh^3(R)}\right) = -l_0\left(\frac{2}{\cosh^2(R)} - \frac{3}{\cosh^4(R)}\right) \tag{22}$$

Solution of the ODE is then achieved through convolution (for the complete solution, see the Appendix, Sect. 6.3):

$$w(t) = \frac{2\pi \sin\left(t\sqrt{2k} - \alpha\sqrt{\frac{2k}{E}}\right)\frac{-l_0}{E+1}\sqrt{\frac{E}{2k}}}{\sinh\left(\pi\sqrt{\frac{k}{2E}}\right)\sqrt{1-\left(\frac{E-1}{E+1}\right)^2}} \left(\begin{array}{l} 2\sinh\left(\sqrt{\frac{k}{2E}}\arccos\left(\frac{E-1}{E+1}\right)\right) \\ + \frac{\frac{E}{E+1}}{1-\left(\frac{E-1}{E+1}\right)^2}\left(\begin{array}{r} 6\frac{E-1}{E+1}\sinh\left(\sqrt{\frac{k}{2E}}\arccos\left(\frac{E-1}{E+1}\right)\right) - \\ 3\sqrt{\frac{2k}{E}\left(1-\left(\frac{E-1}{E+1}\right)^2\right)}\cosh\left(\sqrt{\frac{k}{2E}}\arccos\left(\frac{E-1}{E+1}\right)\right) \end{array}\right) \end{array}\right) \tag{23}$$

where:

$$\alpha = \operatorname{arcsinh}\left(\frac{\sinh\left(x_{1_0} + \frac{l_0}{2}\right)}{\sqrt{E+1}}\right) \tag{24}$$

The residual amplitude can then be simply extracted as:

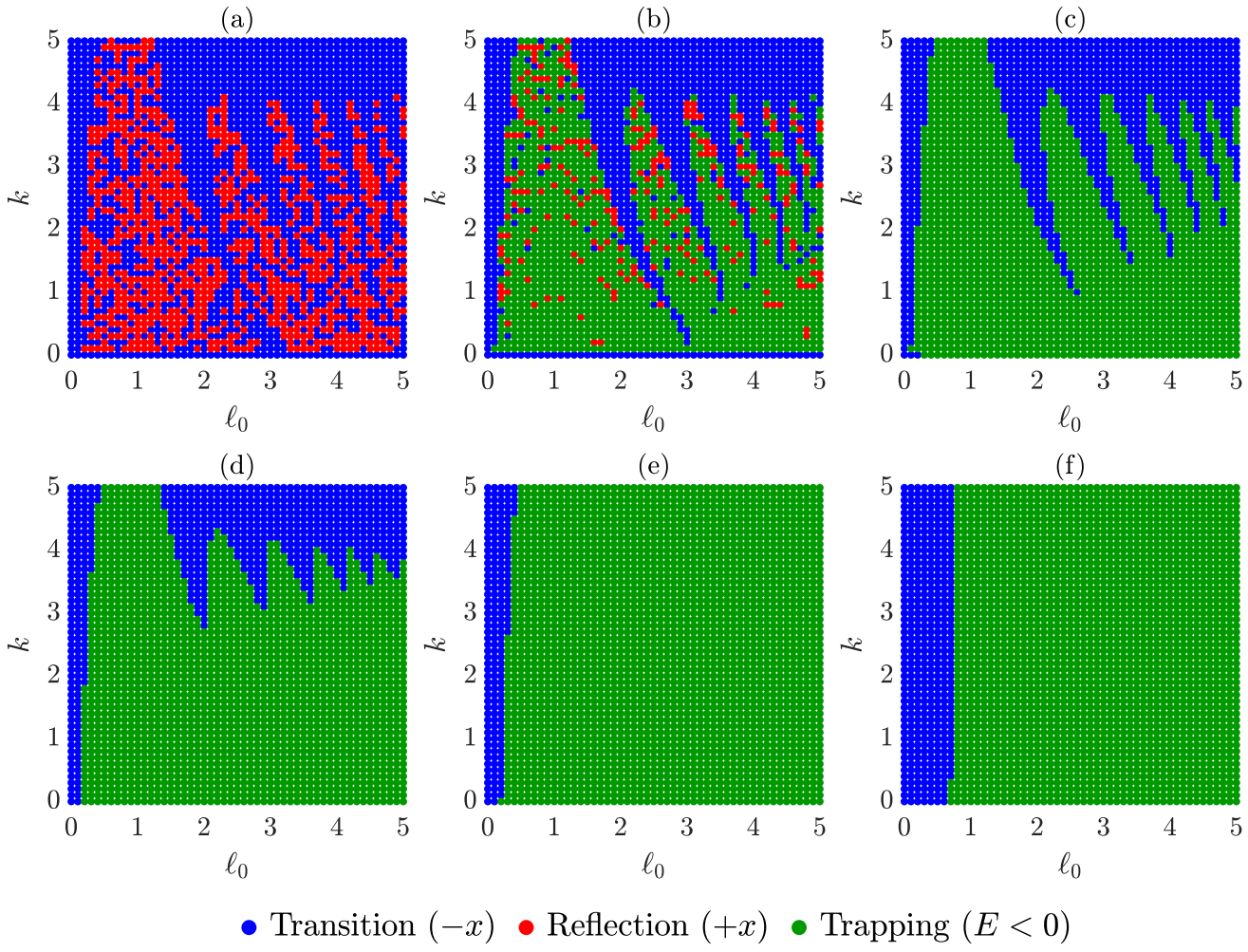

Fig. 7 Scattering and trapping maps for different parameters, the horizontal axis represents the free length l_0 while vertical represents the stiffness k. All maps correspond to the same initial velocity $u_0 = -0.1$. The running parameter is c. **a** $c = 0$ **b** $c = 0.001$ **c** $c = 0.01$ **d** $c = 0.1$ **e** $c = 1$ **f** $c = 10$

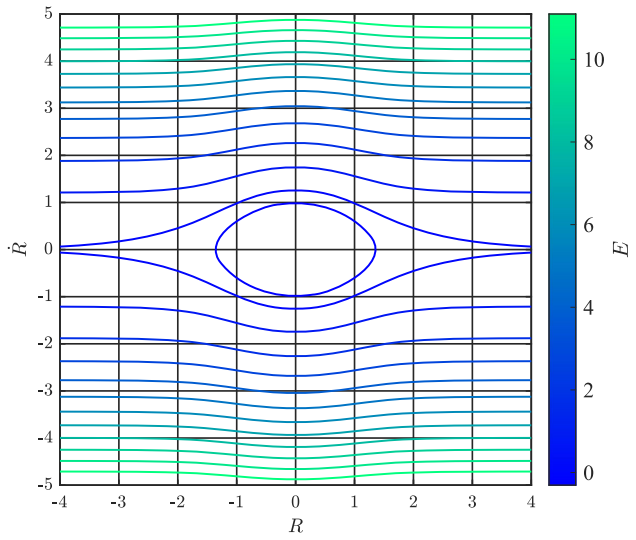

Fig. 8 Phase portrait of the energy equation under the assumption of small oscillations for the free length value $l_0 = 1$

$$amp(w) = \frac{2\pi \frac{-l_0}{E+1}\sqrt{\frac{E}{2k}}}{\sinh\left(\pi\sqrt{\frac{k}{2E}}\right)\sqrt{1-\left(\frac{E-1}{E+1}\right)^2}} \left(2\sinh\left(\sqrt{\frac{k}{2E}}\arccos\left(\frac{E-1}{E+1}\right)\right) + \frac{\frac{E}{E+1}}{1-\left(\frac{E-1}{E+1}\right)^2}\left(6\frac{E-1}{E+1}\sinh\left(\sqrt{\frac{k}{2E}}\arccos\left(\frac{E-1}{E+1}\right)\right) - 3\sqrt{\frac{2k}{E}\left(1-\left(\frac{E-1}{E+1}\right)^2\right)}\cosh\left(\sqrt{\frac{k}{2E}}\arccos\left(\frac{E-1}{E+1}\right)\right)\right)\right) \tag{25}$$

In Figs. 9 and 10 comparisons are plotted between the numerical results and the analytic approximations formulated in Eqs. (17) and (25) for the various parameter regimes. Figure 9 illustrates examples of cases where the "small-free length" approximation provides a better fit, whereas Fig. 10 presents examples where the "large-

velocities" assumption proves to be a better candidate for the approximation. In general, both approximations prove to be viable in their respective regimes and provide a good prediction of the energy transfer trends of the system. As shown in Sect. 3.1, increased lingering inside the well encourages sensitivity. Thus, a disagreement of the numerical solution with the analytic approximations at lower initial velocities is to be expected.

4.3 The threshold of robust scattering outcome

When considering the conservation of energy, the amplitudes given by the analytic approximations (15) and (23) are both expected to converge to zero as the initial energy approaches zero (from the right). As expected, the approximation of large velocities indeed leads to zero residual amplitude under such conditions. However, regarding the "small-free length" approximation, if one were to calculate the same limit, a non-zero expression would be achieved (for the complete derivation, see the Appendix, Sect. 6.4):

$$\lim_{E\to 0^+}(amp(w)) = amp(w_c) = \frac{\pi l_0\left(3\sqrt{2k}-1\right)}{2\sqrt{2k}}e^{-\sqrt{2k}} \tag{26}$$

This result appears somewhat counterintuitive, and upon further investigation, it appears that the system has a certain threshold where numerical results begin to disagree with the assumptions that were made, and the system begins to lose its robustness. The critical initial velocity, the threshold below which the system loses its robustness, is estimated from the condition that when energy is fully transferred into internal oscillations, the amplitude reaches the critical value

$$u_{0_c} = -\sqrt{\frac{k}{2}}amp(w_c) \tag{27}$$

In Fig. 11, graphs of numerical results near the critical velocity confirm that the transition to sensitive behavior occurs around that velocity, serving as a threshold for the robust regime.

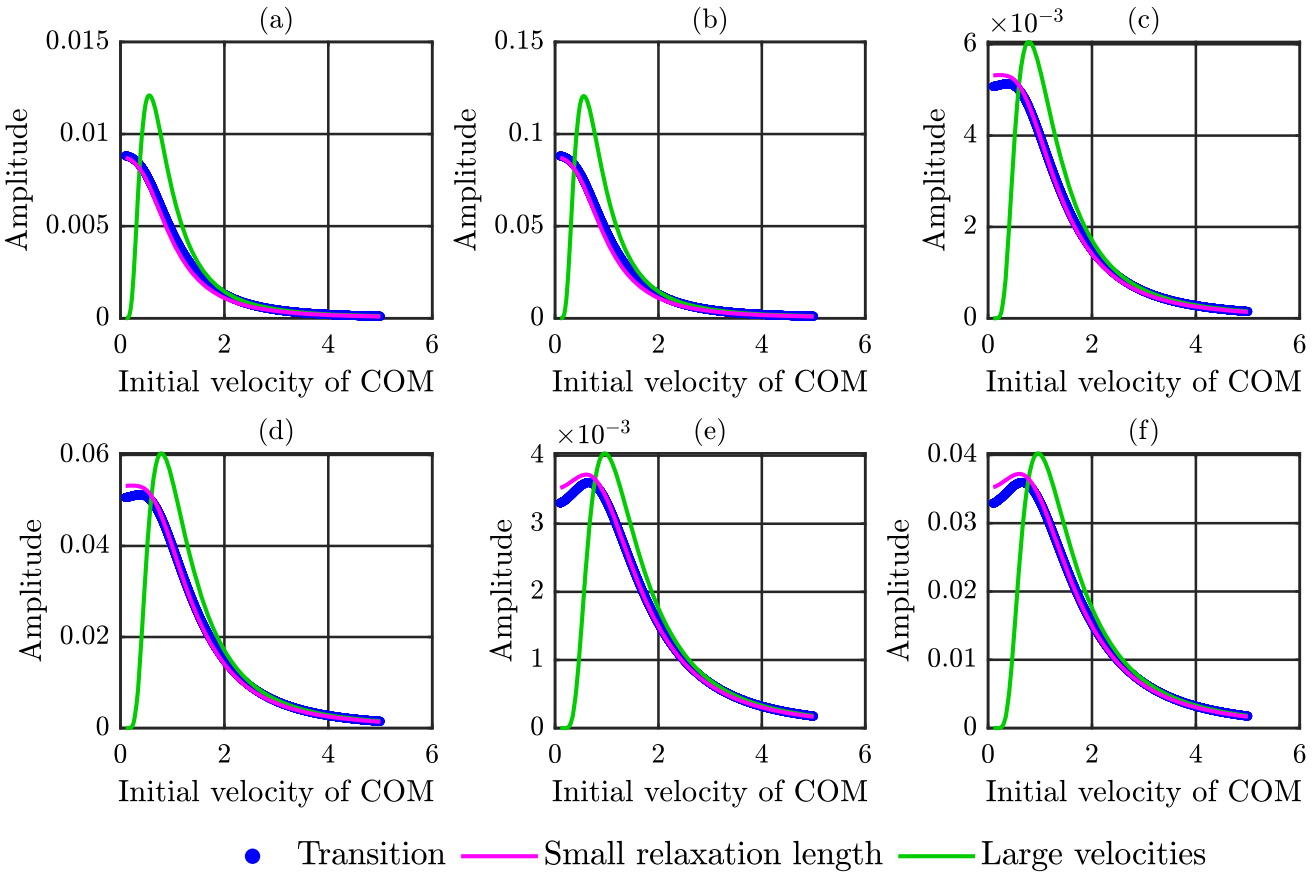

Fig. 9 Comparison of numerical results with analytic approximations of the amplitudes of residual oscillations over the initial velocity for small l_0 values: **a** $l_0 = 0.1, k = 1$ **b** $l_0 = 0.1, k = 2$ **c** $l_0 = 0.1, k = 3$ **d** $l_0 = 0.01, k = 1$ **e** $l_0 = 0.01, k = 2$ **f** $l_0 = 0.01, k = 3$

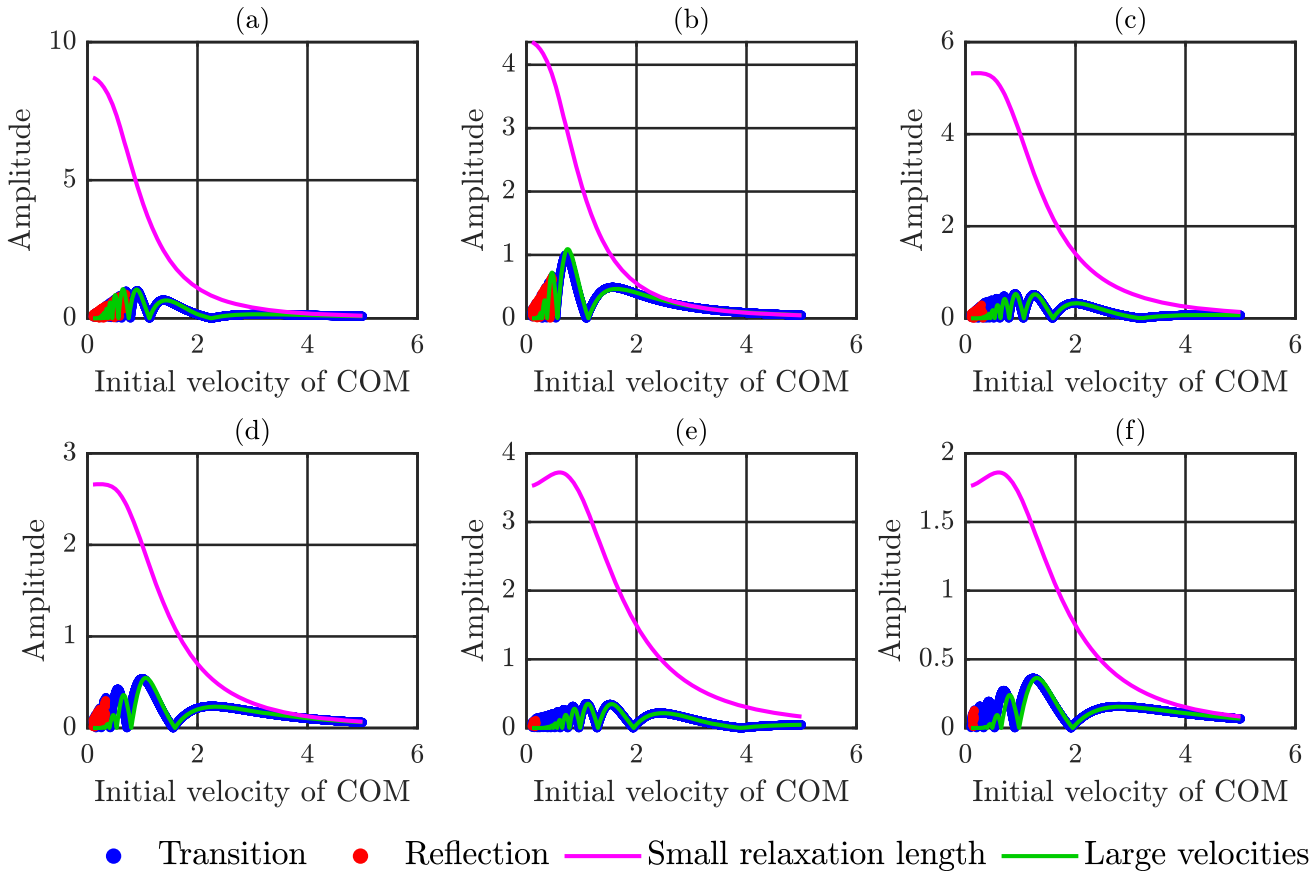

Fig. 10 Comparison of numerical results with analytic approximations of the amplitudes of residual oscillations over initial velocity at large l_0. **a** $l_0 = 5, k = 1$ **b** $l_0 = 5, k = 2$ **c** $l_0 = 5, k = 3$ **d** $l_0 = 10, k = 1$ **e** $l_0 = 10, k = 2$ **f** $l_0 = 10, k = 3$

5 Conclusions

The article focuses on energy exchange trends within the modes of the conservative system. Numerical results showed that such exchange mostly exhibits sensitivity to initial conditions and longer travel time inside the well; however, some asymptotic regimes proved to produce robust results, which were characterized by guaranteed transition and shorter trajectories in the well.

Two approximations for the scattered state amplitude of residual oscillations were formulated, and provided a good fit at their respective regimes, one for the case of large velocities in Eq. (17) and another for the case of small free length values in Eq. (25). The analytical treatment required neglecting the relative displacement mode. Using the latter approximation, we were able to find a threshold value for the initial velocity in Eq. (27), below which the system does not meet the required assumption, thus losing its robustness and displaying reflection.

Given lower energy, the system tended to produce sensitive results, which, with added damping, proved that in such cases, the energy exchange between the modes was encouraged. It seems that as the initial velocity increases, the system tends to lower its energy exchange, thus decreasing the value of the amplitude of residual oscillations. This is, however, not true; the system exhibits a non-monotonous behavior, and the amplitude reaches a certain maximum at robust regimes. The approximations are successful in capturing this non-monotonic behavior of the system.

For future work, it may be interesting to examine the system in higher-dimensional wells, with external damping, or even nonlinear coupling between the particles. Furthermore, exploring the work in applications of engineering (e.g., MEMS, celestial dynamics) is also important.

Appendix A

Full solution of ODE (15)

To solve an ODE with convolution, when considering the equation for w in Eq. (15), we must first obtain the solution for the pulse response of the system:

$$\ddot{w} + 2kw = \delta(t) \tag{28}$$

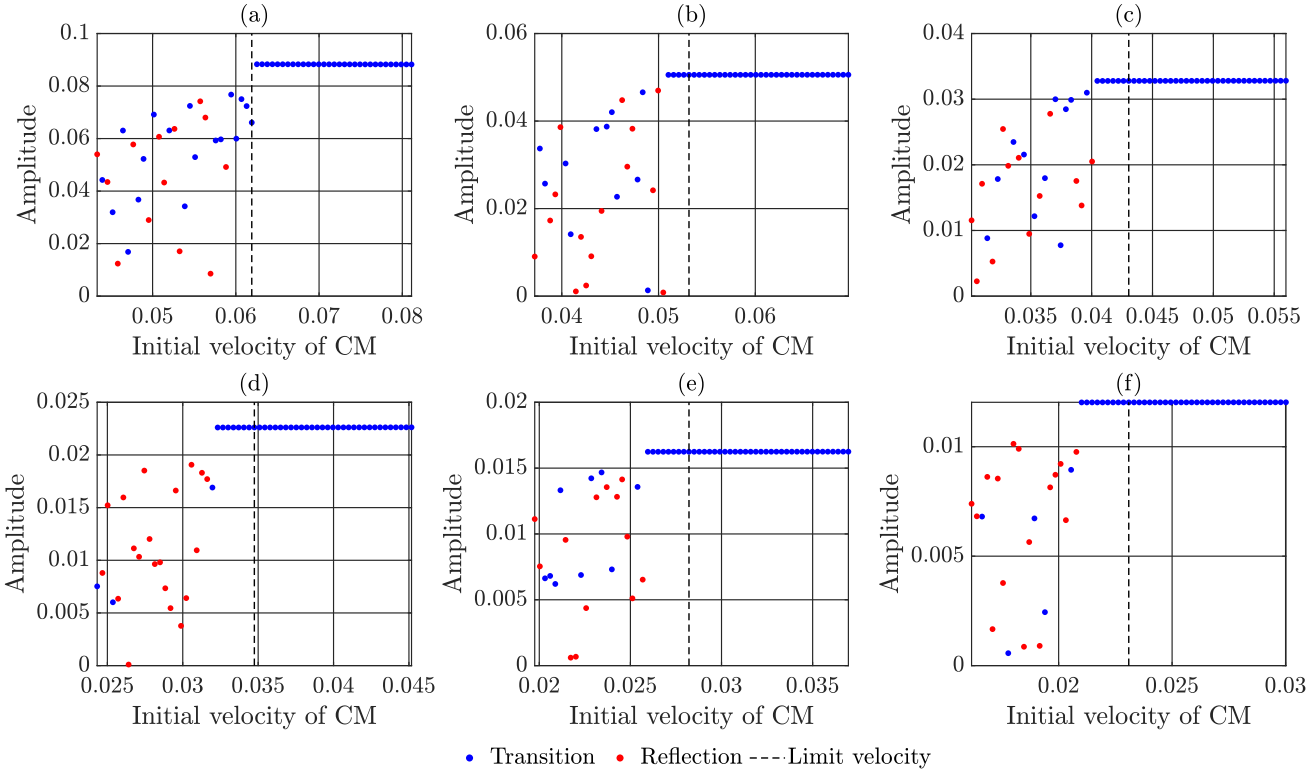

Fig. 11 Amplitude of residual oscillations over initial velocity in the vicinity of the critical velocity, for constant free length $l_0 = 0.1$. **a** $k = 1$ **b** $k = 2$ **c** $k = 3$ **d** $k = 4$ **e** $k = 5$ **f** $k = 6$

The response function is a simple sine with a frequency of $\sqrt{2k}$, which can then be used to formulate the following convolution integral:

$$w(t) = \frac{1}{\sqrt{2k}} \int_{-\infty}^{\infty} \sin\left(\sqrt{2k}(t-\tau)\right) \left(V'\left(x_{1_0} + u_0\tau + \frac{l_0}{2}\right) - V'\left(x_{1_0} + u_0\tau - \frac{l_0}{2}\right)\right) d\tau \tag{29}$$

Trigonometric identities, together with integration by parts, are used to further simplify the calculation:

$$w(t) = \frac{1}{\sqrt{2k}} \sin\left(\sqrt{2k}t\right) \left(\left[\cos\left(\sqrt{2k}\tau\right) V\left(x_{1_0} + u_0\tau + \frac{l_0}{2}\right)\right]_{-\infty}^{\infty} - \left[\cos\left(\sqrt{2k}t\right) V\left(x_{1_0} + u_0\tau - \frac{l_0}{2}\right)\right]_{-\infty}^{\infty} + \int_{-\infty}^{\infty} \sin\left(\sqrt{2k}\tau\right) V\left(x_{1_0} + u_0\tau + \frac{l_0}{2}\right) d\tau - \int_{-\infty}^{\infty} \sin\left(\sqrt{2k}\tau\right) V\left(x_{1_0} + u_0\tau - \frac{l_0}{2}\right) d\tau \right) + \frac{1}{\sqrt{2k}} \cos\left(\sqrt{2k}t\right) \left(\left[\sin\left(\sqrt{2k}\tau\right) V\left(x_{1_0} + u_0\tau - \frac{l_0}{2}\right)\right]_{-\infty}^{\infty} - \left[\sin\left(\sqrt{2k}\tau\right) V\left(u_0\tau + \frac{l_0}{2}\right)\right]_{-\infty}^{\infty} - \int_{-\infty}^{\infty} \cos\left(\sqrt{2k}\tau\right) V\left(x_{1_0} + u_0\tau - \frac{l_0}{2}\right) d\tau + \int_{-\infty}^{\infty} \cos\left(\sqrt{2k}\tau\right) V\left(x_{1_0} + u_0\tau + \frac{l_0}{2}\right) d\tau \right) \tag{30}$$

The force decays exponentially to zero, and all parts outside the integrals can be disregarded:

$$w(t) = \frac{1}{\sqrt{2k}} \sin\left(\sqrt{2k}t\right) \left(\int_{-\infty}^{\infty} \sin\left(\sqrt{2k}\tau\right) V\left(x_{1_0} + u_0\tau + \frac{l_0}{2}\right) d\tau - \int_{-\infty}^{\infty} \sin\left(\sqrt{2k}\tau\right) V\left(x_{1_0} + u_0\tau - \frac{l_0}{2}\right) d\tau \right) + \frac{1}{\sqrt{2k}} \cos\left(\sqrt{2k}t\right) \left(\int_{-\infty}^{\infty} \cos\left(\sqrt{2k}\tau\right) V\left(x_{1_0} + u_0\tau + \frac{l_0}{2}\right) d\tau - \int_{-\infty}^{\infty} \cos\left(\sqrt{2k}\tau\right) V\left(x_{1_0} + u_0\tau - \frac{l_0}{2}\right) d\tau \right) \tag{31}$$

Then, the following variable transformations are applied:

$$\zeta_1 = x_{1_0} + u_0\tau + \frac{l_0}{2}, d\tau = \frac{d\zeta_1}{u_0}$$
$$\zeta_2 = x_{1_0} + u_0\tau - \frac{l_0}{2}, d\tau = \frac{d\zeta_2}{u_0} \tag{32}$$

And with further trigonometric identities, we achieve the following expression:

$$\begin{aligned} w(t) = {} & \frac{1}{u_0\sqrt{2k}}\sin\left(\sqrt{2k}t\right) \\ & \begin{pmatrix} \int_{-\infty}^{\infty} \sin\left(\frac{\sqrt{2k}}{u_0}\left(\zeta_1 - x_{1_0} - \frac{l_0}{2}\right)\right) V(\zeta_1)d\zeta_1 \\ - \int_{-\infty}^{\infty} \sin\left(\frac{\sqrt{2k}}{u_0}\left(\zeta_2 - x_{1_0} + \frac{l_0}{2}\right)\right) V(\zeta_2)d\zeta_2 \end{pmatrix} \\ & + \frac{1}{u_0\sqrt{2k}}\cos\left(\sqrt{2k}t\right) \\ & \begin{pmatrix} \int_{-\infty}^{\infty} \cos\left(\frac{\sqrt{2k}}{u_0}\left(\zeta_1 - x_{1_0} - \frac{l_0}{2}\right)\right) V(\zeta_1)d\zeta_1 \\ - \int_{-\infty}^{\infty} \cos\left(\frac{\sqrt{2k}}{u_0}\left(\zeta_2 - x_{1_0} + \frac{l_0}{2}\right)\right) V(\zeta_2)d\zeta_2 \end{pmatrix} \end{aligned} \tag{33}$$

To avoid long and confusing expressions, each integrand is simplified separately:

$$\begin{aligned} & \int_{-\infty}^{\infty} \sin\left(\frac{\sqrt{2k}}{u_0}\left(\zeta_1 - x_{1_0} - \frac{l_0}{2}\right)\right) V(\zeta_1)d\zeta_1 = \\ & \int_{-\infty}^{\infty} \begin{pmatrix} \sin\left(\frac{\sqrt{2k}}{u_0}\zeta_1\right)\cos\left(\frac{\sqrt{2k}}{u_0}\left(x_{1_0} + \frac{l_0}{2}\right)\right) \\ - \cos\left(\frac{\sqrt{2k}}{u_0}\zeta_1\right)\sin\left(\frac{\sqrt{2k}}{u_0}\left(x_{1_0} + \frac{l_0}{2}\right)\right) \end{pmatrix} V(\zeta_1)d\zeta_1 = \\ & = -\sin\left(\frac{\sqrt{2k}}{u_0}\left(x_{1_0} + \frac{l_0}{2}\right)\right) \int_{-\infty}^{\infty} \cos\left(\frac{\sqrt{2k}}{u_0}\zeta_1\right) V(\zeta_1)d\zeta_1 \end{aligned} \tag{34}$$

$$\begin{aligned} & \int_{-\infty}^{\infty} \sin\left(\frac{\sqrt{2k}}{u_0}\left(\zeta_2 - x_{1_0} + \frac{l_0}{2}\right)\right) V(\zeta_2)d\zeta_2 = \\ & \int_{-\infty}^{\infty} \begin{pmatrix} \sin\left(\frac{\sqrt{2k}}{u_0}\zeta_2\right)\cos\left(\frac{\sqrt{2k}}{u_0}\left(x_{1_0} - \frac{l_0}{2}\right)\right) \\ - \cos\left(\frac{\sqrt{2k}}{u_0}\zeta_2\right)\sin\left(\frac{\sqrt{2k}}{u_0}\left(x_{1_0} - \frac{l_0}{2}\right)\right) \end{pmatrix} V(\zeta_2)d\zeta_2 = \\ & = -\sin\left(\frac{\sqrt{2k}}{u_0}\left(x_{1_0} - \frac{l_0}{2}\right)\right) \int_{-\infty}^{\infty} \cos\left(\frac{\sqrt{2k}}{u_0}\zeta_2\right) V(\zeta_2)d\zeta_2 \end{aligned} \tag{35}$$

$$\begin{aligned} & \int_{-\infty}^{\infty} \cos\left(\frac{\sqrt{2k}}{u_0}\left(\zeta_1 - x_{1_0} - \frac{l_0}{2}\right)\right) V(\zeta_1)d\zeta_1 = \\ & = \int_{-\infty}^{\infty} \begin{pmatrix} \cos\left(\frac{\sqrt{2k}}{u_0}\zeta_1\right)\cos\left(\frac{\sqrt{2k}}{u_0}\left(x_{1_0} + \frac{l_0}{2}\right)\right) \\ + \sin\left(\frac{\sqrt{2k}}{u_0}\zeta_1\right)\sin\left(\frac{\sqrt{2k}}{u_0}\left(x_{1_0} + \frac{l_0}{2}\right)\right) \end{pmatrix} V(\zeta_1)d\zeta_1 = \\ & = \cos\left(\frac{\sqrt{2k}}{u_0}\left(x_{1_0} + \frac{l_0}{2}\right)\right) \int_{-\infty}^{\infty} \cos\left(\frac{\sqrt{2k}}{u_0}\zeta_1\right) V(\zeta_1)d\zeta_1 \end{aligned} \tag{36}$$

$$\begin{aligned} & \int_{-\infty}^{\infty} \cos\left(\frac{\sqrt{2k}}{u_0}\left(\zeta_2 - x_{1_0} + \frac{l_0}{2}\right)\right) V(\zeta_2)d\zeta_2 = \\ & = \int_{-\infty}^{\infty} \begin{pmatrix} \cos\left(\frac{\sqrt{2k}}{u_0}\zeta_2\right)\cos\left(\frac{\sqrt{2k}}{u_0}\left(x_{1_0} - \frac{l_0}{2}\right)\right) + \\ \sin\left(\frac{\sqrt{2k}}{u_0}\zeta_2\right)\sin\left(\frac{\sqrt{2k}}{u_0}\left(x_{1_0} - \frac{l_0}{2}\right)\right) \end{pmatrix} V(\zeta_2)d\zeta_2 = \\ & = \cos\left(\frac{\sqrt{2k}}{u_0}\left(x_{1_0} - \frac{l_0}{2}\right)\right) \int_{-\infty}^{\infty} \cos\left(\frac{\sqrt{2k}}{u_0}\zeta_2\right) V(\zeta_2)d\zeta_2 \end{aligned} \tag{37}$$

Our final expression before integration becomes:

$$\begin{aligned} w(t) = {} & \frac{\sin\left(\sqrt{2k}t\right)}{u_0\sqrt{2k}} \begin{pmatrix} \sin\left(\frac{\sqrt{2k}}{u_0}\left(x_{1_0} - \frac{l_0}{2}\right)\right) \int_{-\infty}^{\infty} \cos\left(\frac{\sqrt{2k}}{u_0}\zeta_2\right) V(\zeta_2)d\zeta_2 - \\ \sin\left(\frac{\sqrt{2k}}{u_0}\left(x_{1_0} + \frac{l_0}{2}\right)\right) \int_{-\infty}^{\infty} \cos\left(\frac{\sqrt{2k}}{u_0}\zeta_1\right) V(\zeta_1)d\zeta_1 \end{pmatrix} \\ & + \frac{\cos\left(\sqrt{2k}t\right)}{u_0\sqrt{2k}} \begin{pmatrix} \cos\left(\frac{\sqrt{2k}}{u_0}\left(x_{1_0} + \frac{l_0}{2}\right)\right) \int_{-\infty}^{\infty} \cos\left(\frac{\sqrt{2k}}{u_0}\zeta_1\right) V(\zeta_1)d\zeta_1 - \\ \cos\left(\frac{\sqrt{2k}}{u_0}\left(x_{1_0} - \frac{l_0}{2}\right)\right) \int_{-\infty}^{\infty} \cos\left(\frac{\sqrt{2k}}{u_0}\zeta_2\right) V(\zeta_2)d\zeta_2 \end{pmatrix} \end{aligned} \tag{38}$$

This expression is relevant for all continuous integrable potentials; in our case, implementing the squared secant potential, a prediction for the amplitude of residual oscillations is achieved:

$$w(t) = \frac{\pi\sqrt{2k}}{u_0^3 \sinh\left(\frac{\pi\sqrt{2k}}{2u_0}\right)} \sin\left(\frac{\sqrt{2k}l_0}{2u_0}\right) \sin\left(\sqrt{2k}t + \frac{\sqrt{2k}}{u_0}\left(x_{1_0} + \frac{l_0}{2}\right)\right) \tag{39}$$

Full solution for the equation of motion (18)

By isolating R and separating the variables, the following expression is obtained:

$$\frac{dR}{\sqrt{E^2 + \frac{1}{\cosh^2(R)}}} = dt \tag{40}$$

The following variable transformation can then be applied:

$$v = \sinh(R),\ \frac{dv}{dR} = \cosh(R) = \sqrt{v^2+1} \tag{41}$$

which simplifies the expression into the following form:

$$\frac{dv}{\sqrt{E(v^2+1)+\frac{1}{2}}} = dt \tag{42}$$

After the integration and isolation of R, the following expression is achieved:

$$R = \operatorname{arcsinh}\left(\sqrt{\frac{E+1}{E}}\cdot\sinh\left(-t\cdot\sqrt{E}+\operatorname{arcsinh}\left(\frac{\sinh\left(x_{1_0}+\frac{l_0}{2}\right)}{\sqrt{E+1}}\right)\right)\right) \tag{43}$$

Solution for the amplitude of the relative oscillations for negligible free length

After applying the assumptions of small free length and negligible amplitudes of residual oscillations, the following relative displacement ODE remains:

$$\ddot{w} + 2kw = -l_0\left(\frac{2}{\cosh^2(R)} - \frac{3}{\cosh^4(R)}\right) \tag{44}$$

We are inserting the expression for R from Eq. (20) and apply the following variable substitution:

$$\zeta = -t\sqrt{E}+\alpha; t = \frac{\alpha-\zeta}{\sqrt{E}} \tag{45}$$

For simplicity, we define

$$\alpha = \operatorname{arcsinh}\left(\frac{\sinh\left(x_{1_0}+\frac{l_0}{2}\right)}{\sqrt{u_0^2+1}}\right) \tag{46}$$

which, after some manipulation, leaves us with the following normalized ODE:

$$w_{\zeta\zeta}+\frac{2k}{E}w = -\frac{l_0}{E}\left(\frac{4E}{(E+1)\left(\frac{E-1}{E+1}+\cosh(2\zeta)\right)} - \frac{12E^2}{(E+1)^2\left(\frac{E-1}{E+1}+\cosh(2\zeta)\right)^2}\right) \tag{47}$$

The impulse response of the system should be considered if one wants to utilize convolution to solve the ODE:

$$w_{\zeta\zeta}+\frac{2k}{E}w = \delta(\zeta) \tag{48}$$

It is rather easy to see that the impulse response in this system is a simple sine with a frequency of $\sqrt{\frac{2k}{E}}$. This result can be utilized to write the convolution integral of the system and thus achieve a solution for the ODE:

$$w(\zeta) = -\frac{l_0}{E}\sqrt{\frac{E}{2k}}\int_{-\infty}^{\infty}\sin\left((\zeta-\tau)\sqrt{\frac{2k}{E}}\right)\left(\frac{4E}{(E+1)\left(\frac{E-1}{E+1}+\cosh(2\tau)\right)} - \frac{12E^2}{(E+1)^2\left(\frac{E-1}{E+1}+\cosh(2\tau)\right)^2}\right)d\tau \tag{49}$$

By applying some trigonometric identities, the integration can be further simplified:

$$w(\zeta) = -\frac{l_0}{\sqrt{2Ek}}\int_{-\infty}^{\infty}\left(\sin\left(\zeta\sqrt{\frac{2k}{E}}\right)\cos\left(\tau\sqrt{\frac{2k}{E}}\right) - \cos\left(\zeta\sqrt{\frac{2k}{E}}\right)\sin\left(\tau\sqrt{\frac{2k}{E}}\right)\right)\left(\frac{4E}{(E+1)\left(\frac{E-1}{E+1}+\cosh(2\tau)\right)} - \frac{12E^2}{(E+1)^2\left(\frac{E-1}{E+1}+\cosh(2\tau)\right)^2}\right)d\tau \tag{50}$$

Some of the terms inside the integration cancel out because they are odd functions integrated over a symmetrical domain, leaving us with two integrals that need to be computed:

$$I_1 = 4\int_{-\infty}^{\infty}\frac{\cos\left(\sqrt{\frac{2k}{E}}\tau\right)}{\frac{E-1}{E+1}+\cosh(2\tau)}d\tau = \frac{4\pi\sinh\left(\sqrt{\frac{k}{2E}}\arccos\left(\frac{E-1}{E+1}\right)\right)}{\sqrt{1-\left(\frac{E-1}{E+1}\right)^2}\sinh\left(\pi\sqrt{\frac{k}{2E}}\right)} \tag{51}$$

$$I_2 = \frac{12E}{E+1}\int_{-\infty}^{\infty}\frac{\cos\left(\sqrt{\frac{2k}{E}}\tau\right)}{\left(\frac{E-1}{E+1}+\cosh(2\tau)\right)^2}d\tau = -\frac{6E}{E+1}\frac{\pi\left(\begin{array}{c}2\frac{E-1}{E+1}\sinh\left(\sqrt{\frac{k}{2E}}\arccos\left(\frac{E-1}{E+1}\right)\right)\\ -\sqrt{\frac{2k}{E}\left(1-\left(\frac{E-1}{E+1}\right)^2\right)}\cosh\left(\sqrt{\frac{k}{2E}}\arccos\left(\frac{E-1}{E+1}\right)\right)\end{array}\right)}{\sinh\left(\pi\sqrt{\frac{k}{2E}}\right)\left(1-\left(\frac{E-1}{E+1}\right)^2\right)^{1.5}} \tag{52}$$

The full solution for the ODE, after inserting Eqs. (51) and (52) into Eq. (50) and transforming the expression back to t is given by

$$w(t)=\frac{2\pi\sin\left(t\sqrt{2k}-\alpha\sqrt{\frac{2k}{E}}\right)\frac{-l_0}{E+1}\sqrt{\frac{E}{2k}}}{\sinh\left(\pi\sqrt{\frac{k}{2E}}\right)\sqrt{1-\left(\frac{E-1}{E+1}\right)^2}}\cdot \left(\begin{array}{l} 2\sinh\left(\sqrt{\frac{k}{2E}}\arccos\left(\frac{E-1}{E+1}\right)\right) \\ +\frac{\frac{E}{E+1}}{1-\left(\frac{E-1}{E+1}\right)^2}\left(\begin{array}{l} 6\frac{E-1}{E+1}\sinh\left(\sqrt{\frac{k}{2E}}\arccos\left(\frac{E-1}{E+1}\right)\right) \\ -3\sqrt{\frac{2k}{E}\left(1-\left(\frac{E-1}{E+1}\right)^2\right)}\cosh\left(\sqrt{\frac{k}{2E}}\arccos\left(\frac{E-1}{E+1}\right)\right) \end{array}\right) \end{array}\right) \tag{53}$$

Limit of the small free length approximation at $E \to 0^+$

In order to obtain the limit of (25) at $E \to 0^+$, one can define the following values:

$$A=\frac{2\sinh\left(\sqrt{\frac{k}{2E}}\arccos\left(\frac{E-1}{E+1}\right)\right)}{\sinh\left(\pi\sqrt{\frac{k}{2E}}\right)}$$

$$B=\frac{E}{E+1}\frac{6\frac{E-1}{E+1}\sinh\left(\sqrt{\frac{k}{2E}}\arccos\left(\frac{E-1}{E+1}\right)\right)}{\sinh\left(\pi\sqrt{\frac{k}{2E}}\right)\left(1-\left(\frac{E-1}{E+1}\right)^2\right)}$$

$$C=\frac{E}{E+1}\frac{3\sqrt{\frac{2k}{E}\left(1-\left(\frac{E-1}{E+1}\right)^2\right)}\cosh\left(\sqrt{\frac{k}{2E}}\arccos\left(\frac{E-1}{E+1}\right)\right)}{\sinh\left(\pi\sqrt{\frac{k}{2E}}\right)\left(1-\left(\frac{E-1}{E+1}\right)^2\right)} \tag{54}$$

Such that

$$amp(w)=\frac{-l_0}{E+1}\sqrt{\frac{E}{2k}}\frac{2\pi}{\sqrt{1-\left(\frac{E-1}{E+1}\right)^2}}(A+B-C) \tag{55}$$

We have to use the approximations at $E \to 0^+$:

$$\frac{E-1}{E+1}=-1+\frac{2E}{E+1}=-1+E+O\left(E^2\right) \tag{56}$$

$$\arccos\left(\frac{E-1}{E+1}\right)=\arccos(-1+2E) \approx \pi-2\sqrt{E}+O\left(E^{1.5}\right) \tag{57}$$

The limit for A is written as follows:

$$\lim_{E\to0^+}A=\lim_{E\to0^+}\frac{2\sinh\left(\sqrt{\frac{k}{2E}}\arccos\left(\frac{E-1}{E+1}\right)\right)}{\sinh\left(\pi\sqrt{\frac{k}{2E}}\right)} =\lim_{E\to0^+}\left(2e^{\sqrt{\frac{k}{2E}}\left(\arccos\left(\frac{E-1}{E+1}\right)-\pi\right)}\frac{1-e^{-2\sqrt{\frac{k}{2E}}\arccos\left(\frac{E-1}{E+1}\right)}}{1-e^{-2\sqrt{\frac{k}{2E}}\pi}}\right)=2e^{-\sqrt{2k}} \tag{58}$$

The limit for B:

$$\lim_{E\to0^+}B=\lim_{E\to0^+}\left(\frac{E}{E+1}\frac{6\frac{E-1}{E+1}\sinh\left(\sqrt{\frac{k}{2E}}\arccos\left(\frac{E-1}{E+1}\right)\right)}{\sinh\left(\pi\sqrt{\frac{k}{2E}}\right)\left(1-\left(\frac{E-1}{E+1}\right)^2\right)}\right)= \lim_{E\to0^+}\left(\frac{6(E-1)\sinh\left(\sqrt{\frac{k}{2E}}\arccos\left(\frac{E-1}{E+1}\right)\right)}{4\sinh\left(\pi\sqrt{\frac{k}{2E}}\right)}\right)= \lim_{E\to0^+}\frac{3(E-1)}{2}\left(e^{\sqrt{\frac{k}{2E}}\left(\arccos\left(\frac{E-1}{E+1}\right)-\pi\right)}\frac{1-e^{-2\sqrt{\frac{k}{2E}}\arccos\left(\frac{E-1}{E+1}\right)}}{1-e^{-2\sqrt{\frac{k}{2E}}\pi}}\right)=-\frac{3}{2}e^{-\sqrt{2k}} \tag{59}$$

The limit for C:

$$\lim_{E\to0^+}C=\lim_{E\to0^+}\left(\frac{E}{E+1}\frac{3\sqrt{\frac{2k}{E}\left(1-\left(\frac{E-1}{E+1}\right)^2\right)}\cosh\left(\sqrt{\frac{k}{2E}}\arccos\left(\frac{E-1}{E+1}\right)\right)}{\sinh\left(\pi\sqrt{\frac{k}{2E}}\right)\left(1-\left(\frac{E-1}{E+1}\right)^2\right)}\right)= \lim_{E\to0^+}\left(\frac{6\sqrt{2k}\cosh\left(\sqrt{\frac{k}{2E}}\arccos\left(\frac{E-1}{E+1}\right)\right)}{4\sinh\left(\pi\sqrt{\frac{k}{2E}}\right)}\right)= \lim_{E\to0^+}\left(\frac{6\sqrt{2k}}{4}\left(2e^{\sqrt{\frac{k}{2E}}\left(\arccos\left(\frac{E-1}{E+1}\right)-\pi\right)}\frac{1+e^{-2\sqrt{\frac{k}{2E}}\arccos\left(\frac{E-1}{E+1}\right)}}{1-e^{-2\sqrt{\frac{k}{2E}}\pi}}\right)\right)=\frac{3}{2}\sqrt{2k}e^{-\sqrt{2k}} \tag{60}$$

Inserting the limits into Eq. (55), we obtain the final result:

$$\lim_{E\to0^+}(amp(w))=\lim_{E\to0^+}\left(\frac{-l_0}{E+1}\sqrt{\frac{E}{2k}}\frac{2\pi}{\sqrt{1-\left(\frac{E-1}{E+1}\right)^2}}(A+B-C)\right)= \lim_{E\to0^+}\left(\frac{-l_0\pi}{\sqrt{2k}}(A+B-C)\right)=\frac{-l_0\pi}{\sqrt{2k}}e^{-\sqrt{2k}}\left(2-\frac{3}{2}-\frac{3}{2}\sqrt{2k}\right)= \frac{l_0\pi}{2\sqrt{2k}}e^{-\sqrt{2k}}\left(3\sqrt{2k}-1\right) \tag{61}$$

Acknowledgements The authors are very grateful to Deutsche Forschungsgemeinschaft (DFG, German Research Foundation) for financial support. Project number: 508244284.

Author Contribution O.G. and Y.A. conceived the work and developed the methodology. Y.A. and A.G. wrote the initial draft. A.G. and A.F prepared revised version, O.G. and A.F. acquired the funding and supervised the work. All authors reviewed the manuscript.

Funding Open access funding provided by Technion - Israel Institute of Technology. Deutsche Forschungsgemeinschaft, 508244284, 508244284, 508244284, 508244284

Data Availability No datasets were generated or analysed during the current study.

Declarations

Conflict of Interest The authors declare no competing interests.

References

1. Ghosh, P.K.: Communication: escape kinetics of self-propelled Janus particles from a cavity: numerical simulations. J. Chem. Phys. (2014). https://doi.org/10.1063/1.4892970
2. Roundy, S., Wright, P.K., Rabaey, J.M.: Energy Scavenging for Wireless Sensor Networks. Springer, New York (2003)
3. Glynne-Jones, P., Tudor, M.J., Beeby, S.P., White, N.M.: An electromagnetic, vibration-powered generator for intelligent sensor systems. Sensors Actuators A Phys. (2004). https://doi.org/10.1016/j.sna.2003.09.045
4. Mann, B.P., Owens, B.A.: Investigations of a nonlinear energy harvester with a bistable potential well. J. Sound Vib. (2010). https://doi.org/10.1016/j.jsv.2009.11.034
5. Andò, B., Baglio, S., Trigona, C., Dumas, N., Latorre, L., Nouet, P.: Nonlinear mechanism in MEMS devices for energy harvesting applications. J. Micromech. Microeng. (2010). https://doi.org/10.1088/0960-1317/20/12/125020
6. Alsaleem, F.M., Younis, M.I., Ruzziconi, L.: An experimental and theoretical investigation of dynamic pull-in in MEMS resonators actuated electrostatically. J. Microelectromech. Syst. (2010). https://doi.org/10.1109/JMEMS.2010.2047846
7. Leus, V., Elata, D.: On the dynamic response of electrostatic MEMS switches. J. Microelectromech. Syst. (2008). https://doi.org/10.1109/JMEMS.2007.908752
8. Marchal, C., Yoshida, J., Yi-Sui, S.: Three-body problem. Celestial Mech. (1984). https://doi.org/10.1007/BF01235792
9. Gómez, G., Koon, W.S., Lo, M.W., Marsden, J.E., Masdemont, J., Ross, S.D.: Connecting orbits and invariant manifolds in the spatial restricted three-body problem. Nonlinearity (2004). https://doi.org/10.1088/0951-7715/17/5/002
10. Duboshin, G.N.: Some remarks on the generalized many-body problem. Celestial Mech. (1972). https://doi.org/10.1007/BF01227824
11. Koon, W.S., Martin, M.W., Marsden, J.E., Ross, S.D.: Heteroclinic connections between periodic orbits and resonance transitions in celestial mechanics. Chaos (2000). https://doi.org/10.1063/1.166509
12. Zotos, E.E.: Escape dynamics and fractal basin boundaries in Seyfert galaxies. Nonlinear Dyn. (2015). https://doi.org/10.1007/s11071-015-1930-7
13. Gendelman, O.V., Karmi, G.: Basic mechanisms of escape of a harmonically forced classical particle from a potential well. Nonlinear Dyn. (2019). https://doi.org/10.1007/s11071-019-04985-9
14. Virgin, L.N., Plaut, R.H., Cheng, C.: Prediction of escape from a potential well under harmonic excitation. Int. J. Non-Linear Mech. (1992). https://doi.org/10.1016/0020-7462(92)90005-R
15. Aguirre, J., Vallejo, J.C., Sanjuán, M.A.F.: Wada basins and chaotic invariant sets in the Hénon-Heiles system. Phys. Rev. E (2001). https://doi.org/10.1103/PhysRevE.64.066208
16. Nayfeh, A.H.: Perturbation Methods. Wiley, Hoboken (2024)
17. Zotos, E.E., Jung, C., Saeed, T.: The basin boundary of the breakup channel in chaotic rearrangement scattering. Nonlinear Dyn. (2021). https://doi.org/10.1007/s11071-021-06240-6
18. Gaspard, P., Rice, S.A.: Scattering from a classically chaotic repellor. J. Chem. Phys. (1989). https://doi.org/10.1063/1.456017
19. Eckhardt, B.: Irregular scattering. Phys. D Nonlinear Phenom. (1988). https://doi.org/10.1016/S0167-2789(98)90012-4
20. Boyd, P.T., McMillan, S.L.: Chaotic scattering in the gravitational three-body problem. Chaos (1993). https://doi.org/10.1063/1.165956
21. Engel, A., Ezra, T., Gendelman, O.V., Fidlin, A.: Escape of two-DOF dynamical system from the potential well. Nonlinear Dyn. (2023). https://doi.org/10.1007/s11071-022-08000-6